

Laser-wakefield accelerators for high-resolution X-ray imaging of complex microstructures

Contact: aehuss@umich.edu

A.E. Hussein, K. Krushelnick

Center for Ultrafast Optical Science, University of Michigan, Ann Arbor, MI 48109-2099, USA

N. Senabulya, A.J. Shahani

Department of Materials Science and Engineering, University of Michigan, Ann Arbor, MI 48109-2099, USA

Y. Ma, M.J.V. Streeter, S.J.D. Dann, O. Finlay,

L. Willingale, A.G.R. Thomas

The Cockcroft Institute, Keckwick Lane, Daresbury, WA4 4AD, UK

B. Kettle, J.M. Cole, E. Gerstmayr, S.P.D. Mangles, Z. Najmudin, J. C. Wood

The John Adams Institute for Accelerator Science, Imperial College London, London, SW7 2AZ, UK

F. Albert, N. Lemos

Lawrence Livermore National Laboratory, NIF and Photon Sciences, Livermore, CA 94550, USA

N. Bourgeois, P.P. Rajeev, D.R. Symes

Central Laser Facility, STFC Rutherford Appleton Laboratory, Didcot OX11 0QX, UK

C.M. Schleputz

Swiss Light Source, Paul Scherrer Institute, CH-5232 Villigen, Switzerland

S. Cipiccia

Diamond Light Source, Harwell Science and Innovation Campus, Fermi Avenue, Didcot OX11 0DE, UK

I. Gallardo González, O. Lundh

Department of Physics, Lund University, P.O. Box 118, S-22100, Lund, Sweden

A. Higginbotham, C. Lumsdon

York Plasma Institute, Department of Physics, University of York, York YO10 5DD, UK

D.A. Jaroszynski, M. Shahzad, R. Spesyvtsev, G. Vieux

SUPA, Department of Physics, University of Strathclyde, Glasgow G4 0NG, UK

K. Falk, M. Smid

ELI Beamline, Institute of Physics of the ASCR, Na Slovance 2, Prague 182 21, Czech Republic

N.C. Lopes

GoLP/Instituto de Plasmas e Fusão

Nuclear, Instituto Superior Técnico

U.L., Lisboa 1049-001, Portugal

Abstract

Laser-wakefield accelerators (LWFAs) are high acceleration-gradient plasma-based particle accelerators capable of producing ultra-relativistic electron beams. Within the strong focusing fields of the wakefield, accelerated electrons undergo betatron oscillations, emitting a bright pulse of X-rays with a micrometer-scale source size that may be used for imaging applications. Non-destructive X-ray phase contrast imaging and tomography of heterogeneous materials can provide insight into their processing, structure, and performance. To demonstrate the imaging capability of X-rays from an LWFA, we have examined an irregular eutectic in the aluminum-silicon (Al-Si) system. The lamellar spacing of the Al-Si eutectic microstructure is on the order of a few micrometers, thus requiring high spatial resolution. An upper bound on the resolving power of $2.7 \pm 0.3 \mu\text{m}$ of the LWFA source in this experiment was measured. These results indicate that betatron X-rays from LWFA can perform high resolution imaging of eutectics and, more broadly, complex microstructures.

1 Introduction

Laser-wakefield acceleration (LWFA) is a method for producing high-energy electron beams using the accelerating field structure produced in the wake of a high-power, ultrashort pulsed laser propagating through low density plasma. During wakefield acceleration, an electron bunch “surfs” on the electric wave generated by the light pressure of an intense laser pulse [1]. This wave induces a strong longitudinal electric field that remains in phase with the relativistic driver, enabling relativistic electrons to gain significant energy from the accelerating field over long distances. Due to the lack of a breakdown limit in a plasma accelerator, accelerating gradients 1000 times stronger than those produced in conventional sources can be produced [1, 2] and the generation of high energy electron beams has been demonstrated experimentally [3–9]. Additionally, in the highly nonlinear regime, electrons undergo betatron oscillations in the strong focusing fields of the wakefield, emitting a bright source of X-rays with a source size as small as one micrometer. [10–12]. Betatron X-ray beams produced *via* LWFA have been shown to produce stable, bright X-ray beams capable of high resolution tomographic imaging [11, 13–17]. The resultant beams have a low divergence (on the order of a few milliradians [18]) and ultrashort

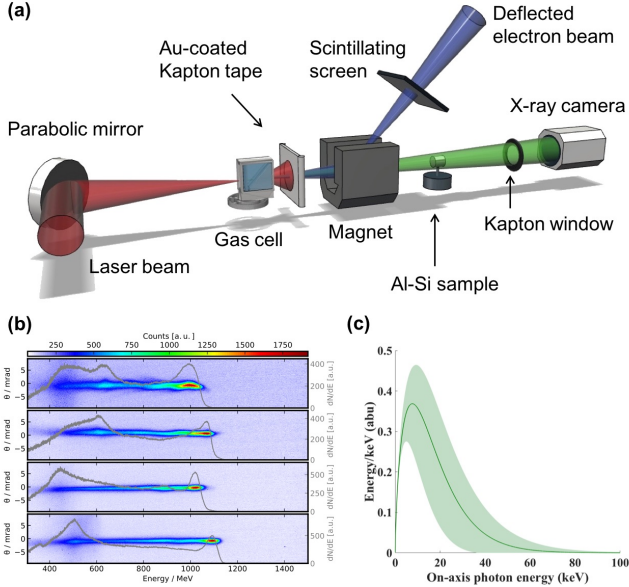


Figure 1: Experimental details for X-ray imaging using a laser wakefield accelerator. (a) Experimental layout. High energy electron and X-ray beams were produced by focusing the beam into a two-stage gas cell. Gold-coated Kapton tape was used to block the laser pulse following the interaction, and was replaced on each shot. A 1 T magnet was used to disperse the electron beam onto a scintillating LANEX screen, from which the electron beam was imaged using a CCD camera. Betatron X-rays passed through the Al-Si sample, which was mounted on a rotation and translation stage at a distance of 19.3 cm from the source. Measurements were made through a kapton vacuum window onto an Andor iKon 2048×2048 pixel CCD camera at a distance of 410 cm from the Al-Si sample. (b) Samples of typical electron beams with a quasi-monoenergetic peak energy and broad low-energy tails. These measurements were obtained at the same experimental conditions as the phase contrast images and betatron spectrum. Electron beam divergence is plotted on the left axis and a line-out of the electron number density (right axis) is overlaid. (c) A best-fit to the betatron X-ray spectrum from an Andor iKon X-ray camera was obtained using a 9-element filter array. Shaded error bars reflect the uncertainty in the critical energy over many shots due to shot-to-shot fluctuations in electron energy.

duration (less than 100 fs [19]), making them useful for a large range of applications across engineering, medicine, homeland security and science [11, 12, 14–17]. Moreover, the demonstration of micrometer scale, keV betatron X-ray beams using a single laser shot demonstrate the potential of these sources for imaging of complex objects in real time using high repetition rate laser systems, enabling X-ray probing with femtosecond resolution [13].

One exciting application for these novel X-ray sources is as a diagnostic tool for additive manufacturing processes. Laser-aided solidification is an avenue of interest in manufacturing science that requires *in situ* measurements with high spatial and temporal resolution [20, 21]. Such is the case for the solidification of eutectics, in which two (or more) solid phases grow simultaneously from a parent liquid phase [22–25]. Once solidified, eutectics act as *in situ* composite materials, providing outstanding mechanical and electrical properties that are not afforded by their constituent phases alone. It is for this reason that lightweight Al-Si alloys comprise over 90% of the total Al parts produced by the United States [26]. Irregular eutectics such as Al-Si are composed of one faceted phase (Si) and another non-faceted (Al) phase. Due to the stiffness of the faceted phase, irregular eutectics feature a non-periodic arrangement of lamellae (fine rods or sheets of adjacent material). The interfacial dynamics underlying irregular eutectic solidification (under relatively low cooling rates) has only recently been elucidated through synchrotron-based X-ray microtomography (denoted XRT), using conventional accelerators. [27]. In general, the lamellar spacing (between Al and Si phases) can be as fine as $1 \mu\text{m}$, thus requiring experimental probes that are capable of delivering high resolution information.

In this report, we investigated the potential of laser-based X-ray sources for the imaging of solid density targets. LWFA experiments were conducted using the Gemini laser. The 40 fs FWHM laser pulse was focused using an $f/40$ parabolic mirror into a gas cell producing an electron beam. A schematic of the experimental setup at the Gemini laser system is given in Figure 1(a). 3D printed two-stage gas cells have been shown to improve the stability, divergence and energy spread of LWFA accelerated electron beams [28], therefore a two-stage gas cell with a 3 mm first stage for injection and a 2 - 21 mm variable length second stage was employed in this experiment. Plasma density was controlled by altering the pressure of the gas supply of each individual stage, and density measurements were made using Stimulated Raman Side Scattering measurements. The plasma density corresponding to the optimum betatron spectrum was $n_p = (4.1 \pm 0.45) \times 10^{18} \text{ cm}^{-3}$ in both stages at a length of 15.5 mm. For these densities, electron beams with average peak energies of $(1000 \pm 150) \text{ MeV}$ were produced. Example electron beams are shown in Figure 1(b), with a superimposed line-out of the spectrum, indicating a quasi-monoenergetic peak and a broad low-

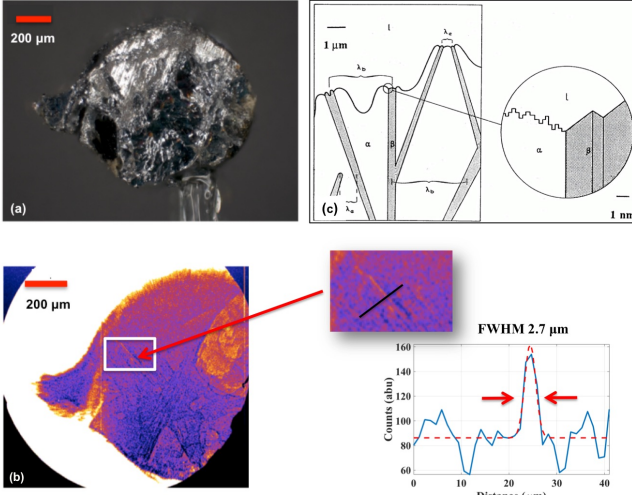


Figure 2: Al-Si sample investigated using a LWFA X-ray source. (a) Optical microscope image of the Al-Si cylindrical sample imaged in LWFA experiments. (b) X-ray phase contrast image obtained with a LWFA, revealing a lamellar microstructure with an interphase spacing on the order of 1 - 3 μm . A line-out from a region of interest in the phase contrast image is shown, indicating $2.7 \pm 0.3 \mu\text{m}$ as an upper bound on the resolving power of this method. (c) A schematic showing growth of irregular eutectics where β represents the faceted phase (e.g., Si), α is the non-faceted, higher volume fraction phase (e.g., Al), and l is the melt ahead of the interface. The microstructure is deemed irregular due to the difficulty or “stiffness” in changing the growth direction of the faceted phase. The inset shows the atomically diffuse α phase and the defect growth mechanism for the faceted β phase. Retrieved with permission from Ref. [29]

energy tail. The X-ray beam, which was assumed to be synchrotron-like as shown in Figure 1(c), contained $1.94 \pm 1.24 \times 10^8$ photons above 5 keV, and is estimated to have a source size smaller than 3 μm , as discussed in *Results*. The LWFA X-ray beam has been found in similar experiments to have divergence on the order of a few millirads [15, 17, 18] and femtosecond duration [16, 19]. The electron and X-ray measurements shown in Figure 1(b) and (c) were not obtained simultaneously, but were taken at identical experimental conditions. In these experiments, the Al-Si sample was 19.3 cm away from the betatron source and an X-ray CCD camera with pixel size of 13.5 μm and a 100 ms exposure time was located 410 cm behind the sample. A total of 136 single-shot images were acquired and no reconstructions were applied.

2 Results

Al-Si samples for phase contrast imaging were prepared by the Materials Preparation Center at Ames Laboratory, with a composition of 50 wt% Si. The larger mass fraction of this primary Si phase in the Al-Si alloy used in these experiments clouded the field-of-view in the X-ray images, limiting the eutectic — which is last to solidify — to a smaller region of the sample. However, this has little to no bearing on the development of the eutectic microstructure. A microscope image of the 1 mm diameter machined sample is shown in Figure 2(a) alongside an example image of the Al-Si microstructure obtained using X-rays from a LWFA in Figure 2(b). The LWFA projection image was obtained using a nearly $22 \times$ magnification, and the banded or lamellar structure can be observed in the zoomed-in image, from which a line-out indicates that the LWFA source is successfully resolving features smaller than 3 μm . The resolution of these images is determined by the geometry of the imaging system. The observed microstructure is consistent with that predicted for irregular eutectics, in which the lamellar spacing can be as fine as 1 μm (Figure 2(c)). In this idealized schematic, the faceted phase β (e.g., Si) and the non-faceted phase α (e.g., Al) are shown, growing in a non-periodic manner into the liquid.

Beyond sharpness and resolution, another consideration in the practical application of LWFA for X-ray imaging is blurring due to the non-zero emission length of the betatron source [30]. Betatron emission is highest at the location of high energy electrons, yielding a very small source size on the order of a few μm [11]. However, the emission length of a betatron source has been found to extend a few millimeters along the axis of laser propagation, resulting in blurring in X-ray images and decreased resolution [30, 31]. This blurring can be observed in Figure 3, where the image resolution is highest near the central axis of the X-ray beam (circled) and begins to blur towards the edges of the sample. It has also been found that the betatron emission length tends to increase with increasing plasma length [31], therefore longer plasma lengths are associated with lower resolution away from the central axis of the laser beam. Additionally, instability in beam pointing can result in variation of the location of highest resolution. For a plasma cell of length 15.5 mm, as employed in these experiments, the emission length of the betatron source was found to be on the order of 5 mm. Image blurring is also a challenge with conventional synchrotron sources, where the emission length can be much longer ($\sim\text{m}$), versus $\sim\text{mm}$ for a LWFA source. However, the large divergence of the LWFA source makes this a concern when the full beam size is used for imaging. It is also important to note that blurring due to the emission length is exacerbated by high magnification. Therefore, the relationship between plasma length and emission can inform optimization of the LWFA X-ray source for high resolution imaging.

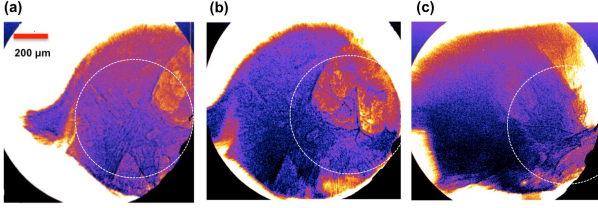


Figure 3: **Blurring of LWFA X-ray images due to finite betatron emission length.** Three LWFA phase contrast images of the Al-Si sample are shown. In (a) and (b) the sample is at the same orientation perpendicular to the laser axis. In image (b) the sample has been translated horizontally by approximately $30 \mu\text{m}$. In (c) the sample has been rotated by 90 degrees about the vertical axis. Regions of sharpest resolution are circled with a dotted line, with a radius of approximately $600 \mu\text{m}$ at highest focus. In all images, blurring can be observed on the order of a millimeter away from the central point due to the emission length of the betatron source. Highest resolution imaging is obtained along the axis of the electron beam; only this section of the image is used for resolution analysis. Blurring due to the emission length of the X-ray source is not unique to betatron sources, also occurring with conventional synchrotron beams, but is exacerbated by high magnification in cases where the full beam is used for imaging.

For high contrast imaging of features in dense materials the critical energy of the X-ray beam must be on the order of several keV. In this experiment, the critical energy of the resultant X-ray beam is determined by comparing the transmission through an array of different elemental filters. The critical energy as a function of plasma density was found to increase with increasing plasma density, as shown in Figure 4(a), reaching a maximum critical energy of nearly 10 keV. These results indicate that LWFA X-ray sources can provide a tunable X-ray source for phase contrast imaging.

The critical photon energy of a LWFA source is related to the maximum energy of the electron beam, γ , and the plasma density, n_p , by [32–34]:

$$E_c = \frac{3}{2} \hbar \omega_\beta K \gamma^2 = \frac{3}{4} \hbar \frac{e^2}{\epsilon_0 m_e c^2} \frac{\sigma}{2} n_p \gamma^2 \quad (1)$$

where $\sigma = 2r_\beta$ is the approximate betatron source size and r_β is the amplitude of betatron oscillations. From equation (1), one can see that the electron energy can be retrieved from the measured critical photon energy, the plasma density n_p and an assumed source size σ using $\gamma \propto \sqrt{2E_c/n_p\sigma}$. Figure 4(b) shows the retrieved electron energies with measured plasma densities and fitted source size σ of (0.2 - 1 μm). A plot of the experimentally measured peak electron energy is superimposed on retrieved electron energies, showing best agreement be-

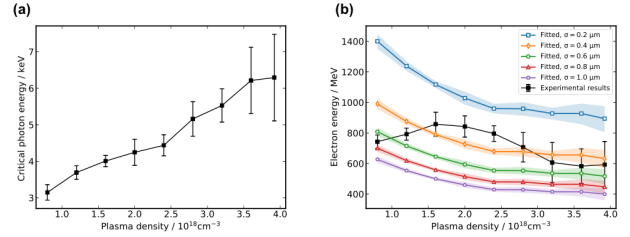


Figure 4: **Critical energy of the LWFA betatron source.** (a) Experimentally measured critical energy of the LWFA X-ray beam as a function of plasma density. (b) Theoretical predictions of the maximum electron energy corresponding to experimentally measured critical energy, shown for betatron source sizes of (0.2 - 1.0) μm along with experimentally measured maximum electron energies in the resultant LWFA beam (black).

tween theory and experimental data for betatron source size on the order of (0.4 - 1.0) μm .

For comparison with experimental results it is important to note that the critical photon energy in equation (1) is mainly determined by the maximum electron energy achieved during acceleration because of the γ^2 scaling. Therefore, the retrieved electron energies represent the maximum electron energies during the acceleration, which are not necessarily the same as those measured from the experiment. This is because for high plasma density (here, $n_p > 1.2 \times 10^{18} \text{cm}^{-3}$) the dephasing length is shorter than the gas cell length and electron beams will experience dephasing. Currently, information about electron dephasing cannot be captured experimentally in a single shot, however novel techniques employing a transverse density gradient may provide single-shot diagnostic information of the temporal evolution of the betatron X-ray spectrum and electron acceleration [35].

3 Conclusion

Our results indicate that betatron X-rays from LWFA can be used for the characterization of eutectic alloys and solid density materials. This opens the door to high-resolution materials diagnostics using laser-based sources, without needing to visit a synchrotron facility. Fine details of the lamellar microstructure were clearly resolved in LWFA projection images (Figure 3(b) inset), indicating an upper bound of $2.7 \mu\text{m}$ on the resolving power of this method. Furthermore, the phase contrast spatial resolution criteria indicate that the LWFA source size may be much smaller than a micrometer, which is corroborated by the theoretical scaling of the betatron energy with plasma density in Figure 4(b) in which the retrieved electron energy was most closely fit assuming betatron source sizes on the order of (0.4 - 1) μm . However, it is important to note that the enhanced spatial

resolution reported in this paper is specific to the experimental conditions of these experiments, and that neither of the two experiments was optimized to obtain the ultimate spatial resolution. The ultrashort exposure time of betatron sources may also provide improved spatial resolution by enabling imaging on a timescale shorter than the frequency of vibrations in experimental setups.

As mentioned in the *Introduction*, one area in which we can demonstrate significant near-term impact of these LWFA sources is through the use of betatron X-rays as a diagnostic tool for real-time monitoring of additive manufacturing. In recent years, additive manufacturing has seen tremendous growth due to developments in processes and materials, as well as a greater understanding of the underlying design principles. It already has huge societal impacts through the ability to produce cheaper and customizable products, such as artificial hips and lightweight aircraft components [36–38]. As-solidified parts have been traditionally characterized by examining their microstructures following manufacturing, however such *post mortem* approaches lack the capability of tracking the interfacial dynamics during the solidification process. In fact, it is well known that quenching distorts the morphology of the solid-liquid interfaces, and thus the micrographs collected following manufacturing do not depict those same interfaces that are present during laser-aided processing. Moreover, the US National Institute of Science and Technology “Measurement Science Roadmap for Metal-Based Additive Manufacturing identifies *in situ* process monitoring and metrology as a key barrier to additive manufacturing implementation [39]. To address this confounding issue, a few investigators have recently employed synchrotron-based X-ray microtomography (denoted XRT) to track the microstructural evolution as a function of time [27, 40]. High-speed synchrotron hard X-ray imaging on the nanosecond timescale has recently been demonstrated [20], however LWFA sources offer temporal resolution on the order of femtoseconds [16, 41, 42]. The realization of high-repetition rate laser drivers for LWFA [43–45] could enable dynamic measurements on an ultra-short timescale. Therefore, the micrometer-scale spatial resolution demonstrated in this paper, combined with femtosecond temporal resolution and high repetition capabilities, indicate that LWFA sources could be used for high-resolution dynamics measurements on an ultra-short timescale.

References

- [1] T. Tajima and J. M. Dawson, *Laser Electron Accelerator*, Physical Review Letters **43**, 215004 (1979).
- [2] E. Esarey, C. B. Schroeder, and W. P. Leemans, *Physics of laser-driven plasma-based electron accelerators*, Reviews of Modern Physics **81**, 1229 (2009).
- [3] A. Modena, Z. Najmudin, A. Dangor, C. Clayton, K. Marsh, C. Joshi, V. Malka, C. Darrow, C. Danson, D. Neely, *et al.*, *Electron acceleration from the breaking of relativistic plasma waves*, Nature **377**, 606 (1995).
- [4] V. Malka, S. Fritzler, E. Lefebvre, M.-M. Amonard, F. Burgy, J.-P. Chambaret, J.-F. Chemin, K. Krushelnick, G. Malka, S. Mangles, *et al.*, *Electron acceleration by a wake field forced by an intense ultrashort laser pulse*, Science **298**, 1596 (2002).
- [5] S. P. D. Mangles, C. D. Murphy, Z. Najmudin, A. Thomas, J. Collier, A. Dangor, E. Divall, P. Foster, J. Gallacher, C. Hooker, D. Jaroszynski, A. Langley, W. Mori, P. Norreys, F. Tsung, R. Viskup, B. Walton, and K. Krushelnick, *Monoenergetic beams of relativistic electrons from intense laser-plasma interactions*, Nature **431**, 535 (2004).
- [6] J. Faure, Y. Glinec, A. Pukhov, S. Kiselev, S. Gordienko, E. Lefebvre, J.-P. Rousseau, F. Burgy, and V. Malka, *A laser-plasma accelerator producing monoenergetic electron beams*, Nature **431**, 541 (2004).
- [7] C. G. R. Geddes, C. Toth, J. van Tilborg, E. Esarey, C. Schroeder, D. Bruhwiler, C. Nieter, J. Cary, and W. Leemans, *High-quality electron beams from a laser wakefield accelerator using plasma-channel guiding*, Nature **431**, 538 (2004).
- [8] W. Leemans, B. Nagler, A. Gonsalves, C. Tóth, K. Nakamura, C. Geddes, E. Esarey, C. Schroeder, and S. Hooker, *GeV electron beams from a centimetre-scale accelerator*, Nature Physics **2**, 696 (2006).
- [9] X. Wang, R. Zgadzaj, N. Fazel, Z. Li, S. Yi, X. Zhang, W. Henderson, Y.-Y. Change, R. Korzekwa, C.-H. Pai, H. Quevedo, G. Dyer, E. Gaul, M. Martinez, A. Bernstein, T. Borger, M. Spinks, M. Donovan, V. Khudik, G. Shevts, T. Ditmire, and M. Downer, *Quasi-monoenergetic laser-plasma acceleration of electrons to 2 GeV*, Nature Communications **4** (2013).
- [10] A. Rousse, K. T. Phuoc, R. Shah, A. Pukhov, E. Lefebvre, V. Malka, S. Kiselev, F. Burgy, J.-P. Rousseau, D. Umstadter, and D. Hulin, *Production of a keV X-Ray beam from synchrotron radiation in relativistic laser-plasma interaction*, Physical Review Letters **93**, 135005 (sep 2004).
- [11] S. Kneip, C. McGuffey, J. L. Martins, S. F. Martins, C. Bellei, V. Chvykov, F. Dollar, R. Fonseca, C. Huntington, G. Kalintchenko, A. Maksimchuk, S. P. D. Mangles, T. Matsuoka, S. R. Nagel, C. A. J. Palmer, J. Schreiber, K. T. Phuoc, A. G. R. Thomas, V. Yanovsky, L. O. Silva, K. Krushelnick, and Z. Najmudin, *Bright spatially coherent*

- synchrotron X-rays from a table-top source*, Nature Physics **6**, 980 (2010).
- [12] F. Albert and A. G. R. Thomas, *Applications of laser wakefield accelerator-based light sources*, Plasma Phys. Control. Fusion **58** (2016).
- [13] S. Fourmaux, S. Corde, K. T. Phuoc, P. Lassonde, G. Lebrun, S. Payeur, F. Martin, S. Sebban, V. Malka, A. Rousse, *et al.*, *Single shot phase contrast imaging using laser-produced Betatron x-ray beams*, Optics Letters **36**, 2426 (2011).
- [14] J. Wenz, S. Schleede, K. Khrennikov, M. Bech, P. Thibault, M. Heigoldt, F. Pfeiffer, and S. Karsch, *Quantitative X-ray phase-contrast microtomography from a compact laser-driven betatron source*, Nature Communications **6**, 7568 (2015).
- [15] J. Cole, J. Wood, N. Lopes, K. Poder, R. Abel, S. Alatabi, J. Bryant, A. Jin, S. Kneip, K. Mecseki, D. Symes, S. Mangles, and Z. Najmudin, *Laser-wakefield accelerators as hard x-ray sources for 3D medical imaging of human bone*, Scientific Reports **5** (2015).
- [16] J. Wood, D. Chapman, K. Poder, N. Lopes, M. Rutherford, T. White, F. Albert, K. Behm, N. Booth, J. Bryant, *et al.*, *Ultrafast Imaging of Laser Driven Shock Waves using Betatron X-rays from a Laser Wakefield Accelerator*, Scientific Reports **8**, 11010 (2018).
- [17] J. M. Cole, D. R. Symes, N. C. Lopes, J. C. Wood, K. Poder, S. Alatabi, S. W. Botchway, P. S. Foster, S. Gratton, S. Johnson, C. Kamperidis, O. Kononenko, M. De Lazzari, C. A. J. Palmer, D. Rusby, J. Sanderson, M. Sandholzer, G. Sarri, Z. Szoke-Kovacs, L. Teboul, J. M. Thompson, J. R. Warwick, H. Westerberg, M. A. Hill, D. P. Norris, S. P. D. Mangles, and Z. Najmudin, *High-resolution μ CT of a mouse embryo using a compact laser-driven X-ray betatron source*, Proceedings of the National Academy of Sciences page. 201802314 (2018).
- [18] F. Albert, B. Pollock, J. L. Shaw, K. Marsh, J. Ralph, Y.-H. Chen, D. Alessi, A. Pak, C. Clayton, S. Glenzer, *et al.*, *Angular dependence of betatron x-ray spectra from a laser-wakefield accelerator*, Physical Review Letters **111**, 235004 (2013).
- [19] B. Mahieu, N. Jourdain, K. T. Phuoc, F. Dorchie, J.-P. Goddet, A. Lifschitz, P. Renaudin, and L. Lecherbourg, *Probing warm dense matter using femtosecond X-ray absorption spectroscopy with a laser-produced betatron source*, Nature Communications **9**, 3276 (2018).
- [20] C. Zhao, K. Fezzaa, R. W. Cunningham, H. Wen, F. De Carlo, L. Chen, A. D. Rollett, and T. Sun, *Real-time monitoring of laser powder bed fusion process using high-speed X-ray imaging and diffraction*, Scientific Reports **7**, 3602 (2017).
- [21] C. L. A. Leung, S. Marussi, R. C. Atwood, M. Towrie, P. J. Withers, and P. D. Lee, *In situ X-ray imaging of defect and molten pool dynamics in laser additive manufacturing*, Nature Communications **9**, 1 (2018).
- [22] K. Jackson and J. D. Hunt, *Lamellae and rod eutectic growth*, Trans. Met. Soc. AIME **236**, 1129 (1966).
- [23] K. Jackson and J. Hunt, *Lamellar and Rod Eutectic Growth*, Vol. 236, pg. 363–376 (1988).
- [24] P. Magnin and R. Trivedi, *Eutectic growth: a modification of the Jackson-Hunt theory*, Acta Metallurgica **39**, 453 (1991).
- [25] J. L. Kang, W. Xu, X. X. Wei, M. Ferry, and J. F. Li, *Solidification behavior of Co-Sn eutectic alloy with Nb addition*, Journal of Alloys and Compounds **695**, 1498 (2017).
- [26] J. R. Davis, *Aluminum and aluminum alloys*, ASM international (1993).
- [27] A. J. Shahani, X. Xiao, and P. W. Voorhees, *The mechanism of eutectic growth in highly anisotropic materials*, Nature Communications **7**, 1 (2016).
- [28] M. Vargas, W. Schumaker, Z. H. He, Z. Zhao, K. Behm, V. Chvykov, B. Hou, K. Krushelnick, A. Maksimchuk, V. Yanovsky, and A. G. Thomas, *Improvements to laser wakefield accelerated electron beam stability, divergence, and energy spread using three-dimensional printed two-stage gas cell targets*, Applied Physics Letters **104** (2014).
- [29] D. J. Fisher and W. Kurz, *A theory of branching limited growth of irregular eutectics*, Acta Metallurgica **28**, 777 (1980).
- [30] S. Corde, C. Thaur, K. T. Phuoc, A. Lifschitz, G. Lambert, J. Faure, O. Lundh, E. Benveniste, A. Ben-Ismaïl, L. Arantchuk, *et al.*, *Mapping the X-ray emission region in a laser-plasma accelerator*, Physical Review Letters **107**, 215004 (2011).
- [31] N. C. Lopes, J. Cole, K. Poder, D. J. Chapman, J. C. Wood, S. Alatabi, E. D. Rutherford, M. E. and, D. R. Symes, S. P. D. Mangles, and Z. Najmudin, *Measurement of the LWFA Betatron source length by cross-correlations over images of granular random targets*, Science and Technology Facilities Council - Central Laser Facility, Annual Report (2015-2016).

- [32] S. Corde, K. T. Phuoc, G. Lambert, R. Fitour, V. Malka, A. Rousse, A. Beck, and E. Lefebvre, *Femtosecond x rays from laser-plasma accelerators*, *Reviews of Modern Physics* **85**, 1 (2013).
- [33] A. G. R. Thomas, *Scalings for radiation from plasma bubbles*, *Physics of Plasmas* **17**, 056708 (2010).
- [34] E. Esarey, B. Shadwick, P. Catravas, and W. Lee-mans, *Synchrotron radiation from electron beams in plasma-focusing channels*, *Physical Review E* **65**, 056505 (2002).
- [35] Y. Ma, D. Seipt, S. Dann, M. Streeter, C. Palmer, L. Willingale, and A. Thomas, *Angular streaking of betatron X-rays in a transverse density gradient laser-wakefield accelerator*, *Physics of Plasmas* **25**, 113105 (2018).
- [36] W. E. Frazier, *Metal Additive Manufacturing: A Review*, *Journal of Materials Engineering and Performance* **23**, 1917 (Jun 2014).
- [37] I. Polozov, V. Sufiiarov, E. Borisov, A. Popovich, and D. Masaylo, *Producing hip implants of titanium alloys by additive manufacturing*, *International Journal of Bioprinting* **2**, 78 (06 2016).
- [38] S. A. Tofail, E. P. Koumoulos, A. Bandyopadhyay, S. Bose, L. O'Donoghue, and C. Charitidis, *Additive manufacturing: scientific and technological challenges, market uptake and opportunities*, *Materials Today* **21**, 22 (2018).
- [39] *US National Institute of Science and Technology Measurement Science Roadmap for Metal-Based Additive Manufacturing*, Energetics Incorporated, Columbia, Maryland (2013).
- [40] S. Moniri and A. J. Shahani, *Chemical modification of degenerate eutectics: A review of recent advances and current issues*, *Journal of Materials Research* pg. 1–15 (2018).
- [41] J.-C. Kieffer, S. Fourmaux, and A. Krol, *The ultrafast high-peak power lasers in future biomedical and medical X-ray imaging*, Vol. 10226, page. 1022612, International Society for Optics and Photonics (2017).
- [42] C. McGuffey, W. Schumaker, T. Matsuoka, V. Chvykov, F. Dollar, G. Kalintchenko, S. Kneip, Z. Najmudin, S. P. Mangles, M. Vargas, V. Yanovsky, A. Maksimchuk, A. G. Thomas, and K. Krushelnick, *On the properties of synchrotron-like X-ray emission from laser wakefield accelerated electron beams*, *Physics of Plasmas* **25** (2018).
- [43] S. Hooker, R. Bartolini, S. Mangles, A. Tünnemann, L. Corner, J. Limpert, A. Seryi, and R. Walczak, *Multi-pulse laser wakefield acceleration: a new route to efficient, high-repetition-rate plasma accelerators and high flux radiation sources*, *Journal of Physics B: Atomic, Molecular and Optical Physics* **47**, 234003 (2014).
- [44] J. Cowley, C. Thornton, C. Arran, R. J. Shalloo, L. Corner, G. Cheung, C. D. Gregory, S. P. Mangles, N. H. Matlis, D. R. Symes, *et al.*, *Excitation and control of plasma wakefields by multiple laser pulses*, *Physical Review Letters* **119**, 044802 (2017).
- [45] D. Gustas, D. Guénot, A. Vernier, S. Dutt, F. Böhle, R. Lopez-Martens, A. Lifschitz, and J. Faure, *High-charge relativistic electron bunches from a kHz laser-plasma accelerator*, *Physical Review Accelerators and Beams* **21**, 013401 (2018).